on a much larger scale than is measurable by the X-ray technique and for these phases to maintain a constancy of local network structure and local agarose concentration. The Pines and Prins work cited earlier appears to support this type of situation, though it must be said that little extra substantiation comes from such electron micrographs as are available or from our own optical microscopy.

Finally, the caveat must be issued that the results obtained here relate to one particular agarose sample, i.e., to one containing a particular degree of structural imperfection in relation to Figure 1 and one having a specific molecular weight distribution. Such factors can cause the extent of hysteresis behavior and other gel properties to vary from sample to sample, but in no way has the present work been able to systematically explore the scope of these variations.

Acknowledgment. We are grateful to our colleagues at the Unilever Research Laboratory, principally P. M. Hart and G. R. Atkins for their advice and assistance in the handling of agarose samples, and as always to L. A. Linger for preparation of the figures. We are also indebted to Drs. J.-P. Busnel and D. Durand of Université du Maine for help in characterizing agarose samples (molecular weight determination). M.D. acknowledges benefit of NATO sponsorship and of the Prix Langlois allocation and thanks the Biopolymer Research Group of Unilever Research Laboratory, Colworth House, for hospitality and support.

Registry No. Agarose, 9012-36-6.

References and Notes

(1) Araki, C. *Bull. Chem. Soc. Jpn.* **1956**, *29*, 543.
(2) Araki, C.; Arai, K. *Bull. Chem. Soc. Jpn.* **1967**, *40*, 1452.
(3) Arnott, S.; Fulmer, A.; Scott, W. E.; Dea, I. C. M.; Moorhouse, R.; Rees, D. A. *J. Mol. Biol.* **1974**, *90*, 269.
(4) Anderson, N. S.; Dolan, T. C. S.; Rees, D. A. *J. Chem. Soc. C.* **1968**, 569.
(5) Rees. D. A. *Chem. Ind.* **1972**, 630.
(6) Dea, I. C. M.; McKinnon, A. A.; Rees, D. A. *J. Mol. Biol.* **1972**, *68*, 153.
(7) Norton, I. T.; Goodall, D. M.; Austen, K. R. J.; Morris, E. R.; Rees, D. A. *Biopolymers* **1986**, *25*, 1009.
(8) Rees, D. A. *Adv. Carbohydr. Chem.* **1969**, *24*, 267.
(9) Rees, D. A. *J. Chem. Soc. B* **1970**, 877.
(10) Obrink, B. *J. Chromatogr.* **1968**, *37*, 329.
(11) Laurent, T. C. *Biochem. Biophys. Acta* **1967**, *136*, 199.
(12) Pines, E.; Prins, W. *Macromolecules* **1973**, *6*, 888.
(13) Miller, W. G.; Kou, L.; Tokyama, K.; Voltaggio, V. *J. Polym. Sci., Poly. Symp. Ed.* **1978**, *65*, 91.
(14) Clark, A. H.; Ross-Murphy, S. B. *Adv. Polym. Sci.* **1987**, *83*, 57.
(15) Busnel, J. P.; Durand, D. Université du Maine, 1987, private communication.
(16) Glatter, O.; Kratky, O. *Small-Angle X-ray Scattering*; Academic: London, 1982.
(17) Reference 16, Chapter 7.
(18) Morris, E. R.; Rees, D. A.; Welsh, E. J.; Dunfield, L. G.; Whittington, S. G. *J. Chem. Soc., Perkin Trans. 2* **1978**, 793.
(19) Amsterdam, A.; Er-el, Z.; Shaltiel, S. *Arch. Biochem. Biophys.* **1975**, *171*, 673.
(20) Coviello, T.; Kajiwara, K.; Burchard, W.; Dentini, M.; Crescenzi, V. *Macromolecules* **1986**, *19*, 2826.
(21) Yanaki, T.; Norisuye, T.; Fujita, H. *Macromolecules* **1980**, *13*, 1462.
(22) Guinier, A.; Fournet, G. *Small-Angle Scattering of X-rays*; Wiley: New York, 1955.
(23) Clark, A. H. Unilever Research, Bedford, U.K., 1987, private communication.
(24) Ter Meer, H.-U.; Burchard, W. In *Integration of Fundamental Polymer Science and Technology*; Kleintjens, L. A., Lemstra, P., Eds.; Elsevier Applied Science: Barking, U.K., 1985; p 230.
(25) Miles, M. J.; Morris, V. J.; Carroll, V.; Wright, D. J.; Bacon, J. R.; Nave, C. *Int. J. Biol. Macromol.* **1984**, *6*, 291.
(26) Watase, M.; Nishinari, K.; Clark, A. H.; Ross-Murphy, S. B., submitted for publication in *Macromolecules*.

Vibrational Spectroscopic Study on Molecular Deformation of Polydiacetylene Single Crystals: Stress and Temperature Dependences of Young's Modulus

Gang Wu, Kohji Tashiro, and Masamichi Kobayashi*

Department of Macromolecular Science, Faculty of Science, Osaka University, Toyonaka, Osaka 560, Japan. *Received July 23, 1987; Revised Manuscript Received March 3, 1988*

ABSTRACT: Resonance Raman and Fourier transform infrared absorption spectra of poly[1,6-di(*N*-carbazolyl)-2,4-hexadiyne] single crystals have been measured under tensile stress σ at various temperatures T, and the σ and T dependences of the vibrational frequencies have been measured for the skeletal modes. The peak positions of these bands were found to shift toward the lower frequency side as the stress increased: $\Delta\tilde{\nu}/\Delta\sigma = -40$ cm^{-1}/GPa for the C≡C stretching mode ν(C≡C), -31 cm^{-1}/GPa for ν(C—C), -5 cm^{-1}/GPa for ν(C═C), and -9 cm^{-1}/GPa for the ∠C—C═C bending mode δ(C—C═C) at room temperature. Such a tendency became more remarkable at higher temperature: $\Delta\tilde{\nu}/\Delta\sigma = -56$ cm^{-1}/GPa for ν(C≡C) and -20 cm^{-1}/GPa for δ(C—C═C) at 210 °C, respectively. By the normal coordinates calculation, variation of the intramolecular force constants with increasing applied stress has been estimated, and then Young's modulus E_l along the chain axis was calculated as a function of σ and T by the lattice dynamical theory. The E_l value calculated for $\sigma = 0$ GPa and $T = 300$ K is 41.1 GPa, in good agreement with the observed value 43.2 GPa. E_l was predicted by theory to exhibit about a 2% decrease per 1 GPa tensile stress at room temperature, while the observed decrement in E_l was about 4.6%/GPa. The calculated E_l was found to decrease by about 0.5% as the temperature increases from 27 to 210 °C, which is too small to reproduce the observed value of about 23.3%. The calculation of the atomic displacements and the potential energy distribution in the mechanically deformed polyDCHD chain showed that such a large discrepancy between the observed and calculated σ–T dependence of E_l was ascribed to the neglect of a significant contribution of such a vibrational mode as skeletal torsional motion, the band corresponding to this mode being hardly detected by the present FTIR and resonance Raman spectroscopy. The vibrational coupling between the resonant skeletal and off-resonant side-group modes was observed for some Raman bands, which was analyzed on the basis of the perturbation theory.

Introduction

In order to understand the mechanical properties of crystalline polymers from the molecular theoretical point of view, it is necessary to detect directly the changes in structure and intra- and intermolecular interactions induced by the externally applied stress and strain.

0024-9297/89/2222-0188$01.50/0

Whenever we try to perform such a measurement, however, we always encounter a very serious problem concerning the distribution of the applied stress within the bulk samples. The experimental results are difficult to interpret in a quantitative fashion by the widely used simple model of homogeneous stress distribution, due to the complicated mechanical coupling between the crystalline and amorphous phases.[1] Therefore it is necessary to utilize polymer samples consisting only of a crystalline phase, i.e., polymer single crystals. The generally obtainable polymer single crystals are only of micron or submicron order and so cannot be handled with the usual instruments. (Only one exception has been reported so far. Geil et al.[2] measured the stress–strain curve of polyethylene single crystal by using a specially designed "nanotensilometer".) One of the most promising candidates for such a purpose may be polydiacetylene (PDA). PDA single crystals are obtained by solid-state polymerization and have a needlelike shape with a size of several millimeters to a few centimeters in length.[3]

Investigation of the elastic behavior of PDA single crystals at the molecular level has been made mainly based on the Raman spectroscopic measurement under tension at room temperature.[4-6] The frequency shift of the Raman bands was measured as a function of tensile strain. The data were interpreted in terms of anharmonicity or the stress–strain dependence of the intramolecular force constants, especially for the skeletal stretching and bending modes.[4,5] Such an experiment can make us expect that Young's modulus will be also influenced by the externally applied force through the anharmonic effect of the potential. The effect of temperature variation will be also important because the potential field may be influenced by the thermally induced anharmonicity as well as the thermally activated molecular motion.[7]

In the present paper we will report the Raman and infrared spectral change of a PDA single crystal under tension at various temperatures, from which the stress and temperature dependence of Young's modulus will be estimated on the basis of the lattice dynamical theory.[8] The results will be compared with the mechanical data measured on the bulk PDA single crystal. The atomic displacements induced by the external stress and the strain energy distribution among the internal coordinates such as bond length, bond angle, etc. will be also calculated and compared with the vibrational spectral data measured under tension.

Experimental Section

Sample. In this study, poly[1,6-di(*N*-carbazolyl)-2,4-hexadiyne] (abbreviated as polyDCHD) single crystals[9] were utilized. This has the chemical structure

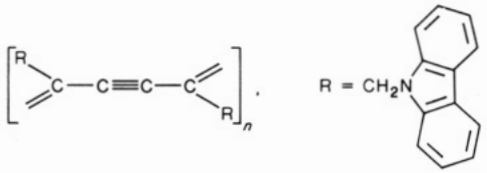

DCHD monomer was recrystallized slowly from a toluene solution to obtain a large needlelike single crystal (Figure 1). The monomer single crystal was polymerized in a solid state by the irradiation of ^{60}Co γ-ray (40 Mrad) at room temperature. Thus obtained polyDCHD single crystal had a needlelike shape with dimensions of 30 mm long and 0.1 mm wide (Figure 1). The cross-sectional area of the crystal is required to be as homogeneous as possible to give a uniform stress over the whole sample. The apparently uniform single crystals were picked out under the optical microscope and supplied for the spectroscopic measurement as well as the stress–strain measurement. In Figure 1 are

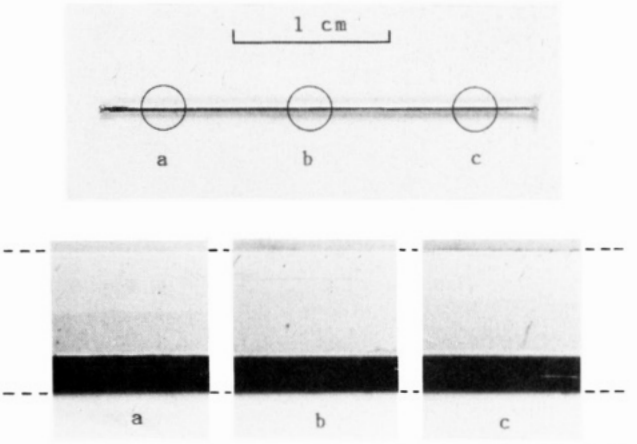

Figure 1. Optical microscopic photographs of a polyDCHD single crystal.

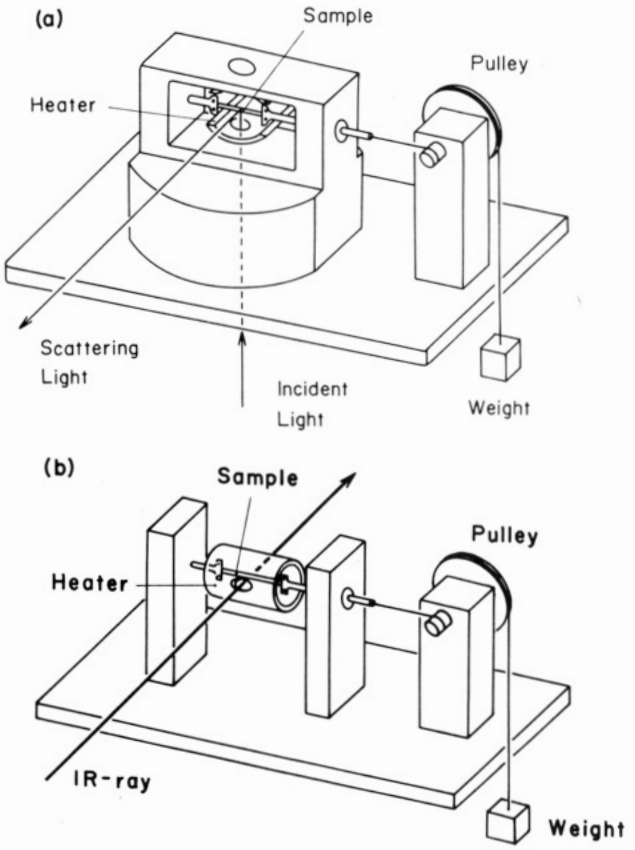

Figure 2. Schematic diagrams of (a) Raman spectral and (b) FTIR spectral measuring systems under stress.

given also the microscope photographs taken for various parts of the single crystal, showing a relatively uniform thickness along the chain axis of the sample. (The fluctuation of the cross-sectional area along the needle crystal is estimated to be less than 3%.) The cross-sectional area of the single crystal was calculated from the weight, length, and density of the crystal. Strictly speaking, the cross-sectional area will be changed from the initial value by the so-called Poisson's effect under tensile stress as well as by the thermal expansion effect. But these changes are estimated to be only 1–2% in the stress and temperature regions employed in the present study. The stress variation may be on the order of 1–2% at most, which will be neglected here in a good approximation.

Raman Spectral Measurements under Tension. For the Raman spectral measurements under tension at various temperatures, we developed an optical cell shown in Figure 2a. The sample was set horizontally. One end of the sample was fixed at the holder and the other end was drawn by applying a weight

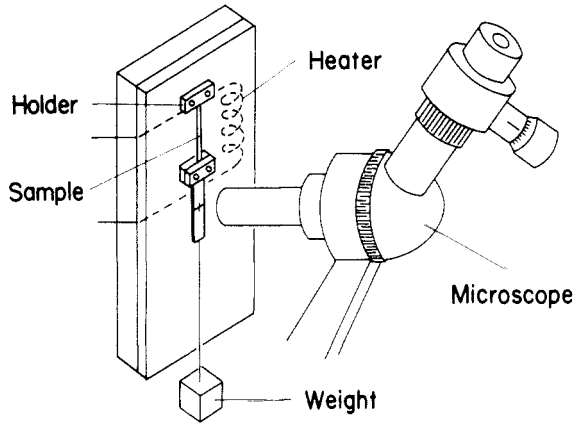

Figure 3. Schematic diagram of the stress–strain measuring system.

through a set of pulleys, which could enlarge a small weight to the larger force by the principle of a lever. The stress was calculated by dividing the applied weight by the cross-sectional area of the sample. The sample was heated with a flexible heater surrounding it. The temperature was monitored by a chromel–alumel thermocouple and controlled within ±1–2 °C. The polarized Raman spectra were measured with a 90° scattering geometry. The visible and ultraviolet absorption spectra of polyDCHD were found to show an absorption peak near the wavelength of 662 nm.[10] Then the resonance Raman spectra were observed by using the 632.8-nm line from a He–Ne gas laser as the excitation light. The Raman spectra were taken with a Japan Spectroscopic Co. R800 Raman spectrophotometer.

FTIR Spectral Measurements under Tension. Fourier-transform infrared (FTIR) spectra of a polyDCHD single crystal were measured in transmission. A single crystal was set onto the drawing apparatus shown in Figure 2b and a constant weight was loaded. In order to prevent the infrared beam from leaking out of the sample, the single crystal was covered with an aluminium foil having a narrow slit. Polarized spectra at various temperatures were measured with a JASCO FT/IR-5MP spectrophotometer.

Stress–Strain Curves. The stress–strain curves of polyDCHD single crystals were measured in a static mode. As shown in Figure 3, a needlelike crystal was hung down vertically with a weight applied. The extension of the sample length was measured by direct observation under the optical microscope.

Results and Discussion

Normal Coordinate Treatment of PolyDCHD Single Chains. PolyDCHD single chains have a fully extended conformation with one-dimensional space group whose factor group is isomorphous to the point group C_{2h}.[11] The zone-center normal modes are classified into the following four symmetry species: A_g, Raman active (α_{xx}, α_{yy}, α_{zz}, α_{yz}), n = 8; B_g, Raman active (α_{xy}, α_{zx}), n = 3; A_u, IR active (μ_x), n = 3; B_u; IR active (μ_y, μ_z), n = 6, where the z axis is along the chain axis and the xz plane is parallel to the zigzag plane. μ and α are transitional dipole moment and polarizability tensor components, respectively, and n is the number of modes belonging to each species. Figure 4 shows the polarized resonance Raman spectra of polyDCHD single crystals measured under tension-free conditions at room temperature. Most of the observed Raman bands have (zz) polarization and are assigned to the A_g symmetry species. Referring to the behavior of these Raman bands under tension (discussed later), the bands at 2081, 1468, 1220, and 985 cm^{-1} can be tentatively assigned to the vibrational modes of ν(C≡C), ν(C=C), δ(C—C=C), and δ(C—C≡C), respectively, where ν denotes the bond stretching mode and δ the bending mode.[5,12]

In order to confirm this assignment, we calculated the normal mode frequencies for a simple model shown in Figure 5. The side group $CH_2NC_{12}H_8$ is simplified as X–Y,

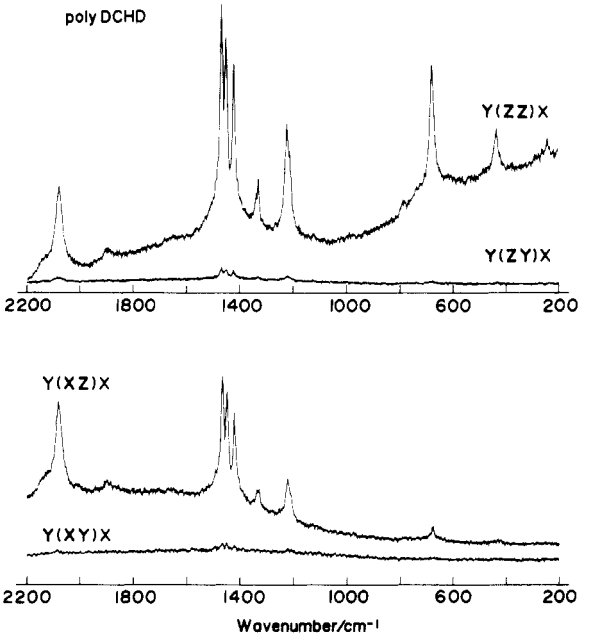

Figure 4. Polarized Raman spectra of a polyDCHD single crystal.

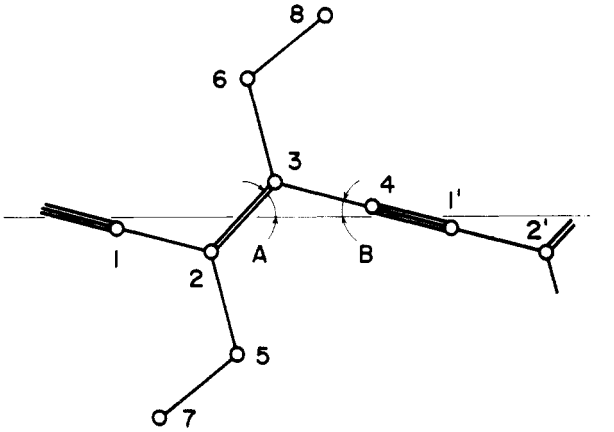

Figure 5. Structural model of polyDCHD used to calculate the normal mode vibrations.

where X and Y denote the CH_2 and carbazolyl groups, respectively. The interatomic distances and bond angles are as follows[5] (refer to Figure 5): $r_{12} = r_{34}$ = 0.143 nm, r_{23} = 0.136 nm, $r_{41'}$ = 0.119 nm, $r_{25} = r_{36}$ = 0.151 nm, $r_{57} = r_{68}$ = 0.147 nm, $\angle A$ = 46°, $\angle B$ = 14°, $\angle 213 = \angle 215 = \angle 235 = \angle 324 = \angle 326 = \angle 346$ = 120°, $\angle 431' = \angle 1'42'$ = 180°, and $\angle 527 = \angle 638$ = 111°. For the intramolecular interactions, the valence force field was adopted, where only the diagonal force constants of the bond stretching and bond angle deformation were taken into consideration and the off-diagonal components were neglected for simplicity. Although such an approximation is thought to be rather rough, the calculated results of the vibrational frequencies and potential energy distribution are not so unreasonable. The force constants reported by Batchelder and Bloor[5] were utilized with some modification: for the bond stretching, K(C—C) = $K_{12} = K_{34}$ = 5.6, K'(C—C) = $K_{57} = K_{68}$ = 4.5, K''(C—C) = $K_{25} = K_{36}$ = 3.0, K(C=C) = K_{23} = 5.1, and K(C≡C) = $K_{41'}$ = 11.7 (in unit of 10^2 N m^{-1}), and for the bond angle deformation, H(C—C≡C) = $H_{341'}$ = 1.42, H(C—C=C) = $H_{213} = H_{235} = H_{324} = H_{326}$ = 0.56, H(C—C—C) = $H_{215} = H_{345}$ = 0.62, and H'(C—C—C) = $H_{257} = H_{368}$ = 0.47 (in unit of 10^2 Nm rad^{-2}), where the subscripts denote the atom numbers shown in Figure 5.

The normal mode frequencies were calculated by the GF matrix method based on the Cartesian coordinate system.[13]

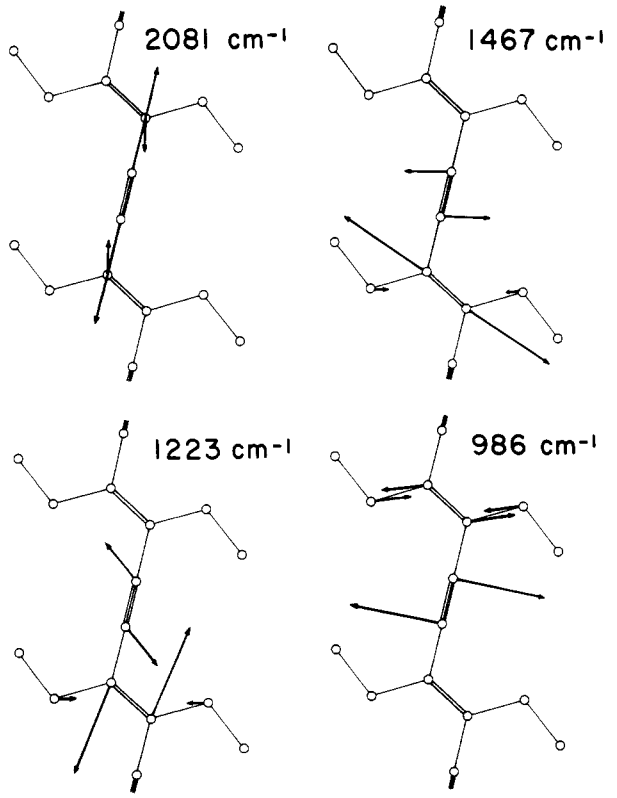

Figure 6. Calculated atomic displacements for the Raman-active skeletal modes of a polyDCHD single chain.

Table I
Calculated Potential Energy Distribution for Some Vibrational Modes Related to the Molecular Skeleton

calcd vibratnl freq, cm^{-1}	potential energy distribution, %				
	ν(C≡C)	ν(C=C)	ν(C—C)	δ(C—C=C)	δ(C—C≡C)
2081 (A_g)	70	1	28	0	0
1467 (A_g)	2	51	1	5	22
1307 (B_u)	0	0	88	0	0
1223 (A_g)	15	9	19	12	11
986 (A_g)	1	10	1	0	57

The calculated frequencies of the four skeletal vibrational modes under free tension are 2081, 1467, 1223, and 986 cm^{-1}, in excellent agreement with the observed values 2081, 1468, 1220, and 985 cm^{-1}, respectively. Strictly speaking, the observed frequencies of ν(C=C) and δ(C—C=C) modes should be corrected to 1462 and 1217 cm^{-1}, respectively, because the vibrational coupling with the side-group modes affects these modes more or less. The detailed analysis will be described in a later section. Figure 6 illustrates the atomic displacements in each vibrational mode. In Table I is shown the potential energy distribution for these vibrational modes. It should be noted here that the 1220-cm^{-1} band consists of the coupling of many components including ν(C≡C), ν(C=C), ν(C—C), δ(C—C=C), and δ(C—C≡C) as seen in this table. But the calculated atomic displacements in Figure 6 allow us to denote this band as δ(C—C=C) in an approximation because the displacement vectors of the carbon atoms of the C=C bond are overwhelmingly large compared with the other ones.

The actually observed Raman spectra include many other bands not assignable by the present simple model. For example, the bands at 1450, 1422, 1328, 676, and 434 cm^{-1} may come from the vibrational modes of the complicated side group consisting of methylene and carbazolyl ring. These modes are considered to be originally in an off-resonance state for the 632.8-nm excitation beam. But,

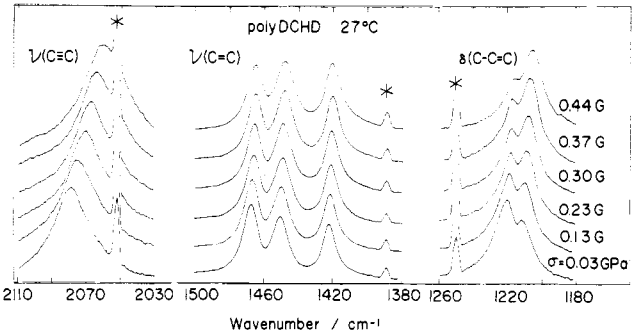

Figure 7. Stress dependence of the Raman spectra measured for the ν(C≡C), ν(C=C), and δ(C—C=C) bands of polyDCHD at 27 °C. Asterisks are due to the emission from a neon lamp.

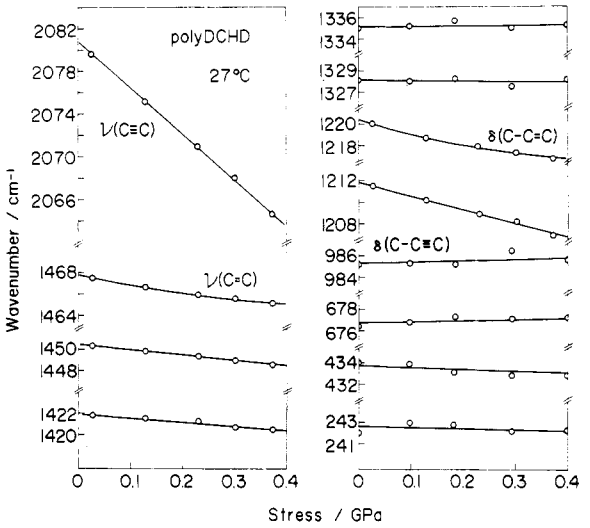

Figure 8. Stress dependence of vibrational frequencies for all the Raman-active bands observed for a polyDCHD single crystal.

due to the vibrational coupling with the skeletal conjugated system, they are considered to "borrow" a part of vibrational intensity from the skeletal modes and are observed in the Raman spectra with rather high intensity. Details will be discussed later.

Polarized Raman and FTIR Spectra Measured under Tension at Room Temperature. A. Raman Spectral Change. As mentioned in the previous section, the Raman bands at 2081, 1468, 1220, and 985 cm^{-1} are approximately assigned to the stretching and bending modes related to the triple and double bonds [ν(C≡C), ν(C=C), δ(C—C=C), and δ(C—C≡C), respectively]. Figure 7 shows the Raman spectral change induced by the tensile stress. The bands indicated by asterisks are due to the emission from a neon lamp located near the entrance slit of the spectrophotometer, which was used as a wavenumber standard. Figure 8 shows the stress dependence of the vibrational frequencies. Among all the bands observed in Raman spectra, the bands at 2081, 1468, and 1220 cm^{-1} are found to show relatively large low-frequency shifts by the application of stress: the frequency shifts were −40, −5, and −9 cm^{-1}/GPa, respectively. The bands originating from the side groups (1328, 676, 434 cm^{-1} etc.) do not shift notably within the experimental error.

The overlapped bands locating near 1220 cm^{-1} change their relative intensity as the tensile stress increases. This may be due to the change in the vibrational coupling between the skeletal deformation band (1220 cm^{-1}) and the side-group band (1212 cm^{-1}) possibly of the carbazolyl ring. A set of the bands around 1450 cm^{-1} are also found to change their relative intensity and position with stress, though not so largely. By referring to the spectral patterns

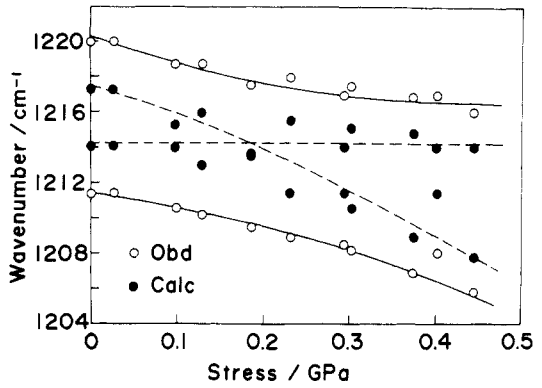

Figure 9. Stress dependence of peak frequencies of the coupled bands in the region 1200–1220 cm^{-1} (open circles). The solid circles represent the behavior of the unperturbed modes calculated from the data of the open circles.

of the carbazole and *N*-ethylcarbazole, the bands at 1450 and 1422 cm^{-1} may be assigned to the CH_2 bending mode and the ring stretching mode of the carbazolyl group, respectively. The frequency shift of these bands is considered to be due to the vibrational coupling with the skeletal C=C stretching mode (1468 cm^{-1}), as described in the previous section. Batchelder et al. analyzed a similar spectral change observed for poly[1,6-bis[*p*-tolylsulfonyl)oxy]-2,4-hexadiyne] (polyTS) by the perturbation theory on the vibrational coupling.[5] In this section, we will try to analyze quantitatively the present experimental data by their method.

As is well-known, the perturbation theory gives the vibrational levels of the coupled two modes by the following equations.

$$\tilde{\nu}_i' = \tfrac{1}{2}[\tilde{\nu}_1^0 + \tilde{\nu}_2^0 \pm (\delta^2 + 4|\tilde{W}_{12}|^2)^{1/2}] \quad (+, i = 1; -, i = 2) \quad (1)$$

where δ is defined as

$$\delta = \tilde{\nu}_1^0 - \tilde{\nu}_2^0 \quad (2)$$

and $\tilde{W}_{12}$ is a perturbation energy. The superscript "0" denotes the unperturbed state. If the unperturbed mode 2 is in an off-resonance state and gives rise to a negligibly small Raman intensity, then the relative intensity ratio of the two Raman bands is expressed by

$$R = I_2/I_1 = \frac{(\delta^2 + 4|\tilde{W}_{12}|^2)^{1/2} - \delta}{(\delta^2 + 4|\tilde{W}_{12}|^2)^{1/2} + \delta} \quad (3)$$

The frequency $\tilde{\nu}_1^0$ (and $\tilde{\nu}_2^0$) is shifted under tension and so δ is a function of stress. If the $\tilde{\nu}_1^0$ and $\tilde{\nu}_2^0$ are accidentally equal to each other at a given stress σ^*, then $\delta = 0$ and the intensity ratio R becomes unity, just when the frequency gap between the two bands is given by

$$\tilde{\nu}_1'(\sigma^*) - \tilde{\nu}_2'(\sigma^*) = 2|\tilde{W}_{12}| \quad (4)$$

Therefore if we can measure the stress σ^* when the relative intensities of the coupled bands become equal to each other [$R(\sigma^*) = 1$], the perturbation energy $|\tilde{W}_{12}|$ can be obtained from eq 4 by measuring the frequency difference of the actually observed two bands. When such a condition of $R = 1$ is not observed, the $|\tilde{W}_{12}|$ may be obtained by least-squares fitting of the observed data of R, $\tilde{\nu}_1'$, and $\tilde{\nu}_2'$. From the thus obtained $|\tilde{W}_{12}|$, the intrinsic "unperturbed" frequencies $\tilde{\nu}_1^0$ and $\tilde{\nu}_2^0$, as a function of stress σ, can be obtained as follows. From eq 1

$$\tilde{\nu}_1^0 = \tfrac{1}{2}[\tilde{\nu}_1' + \tilde{\nu}_2' + [(\tilde{\nu}_1' - \tilde{\nu}_2')^2 - 4|\tilde{W}_{12}|^2]^{1/2}] \quad (5)$$

$$\tilde{\nu}_2^0 = \tfrac{1}{2}[\tilde{\nu}_1' + \tilde{\nu}_2' - [(\tilde{\nu}_1' - \tilde{\nu}_2')^2 - 4|\tilde{W}_{12}|^2]^{1/2}] \quad (6)$$

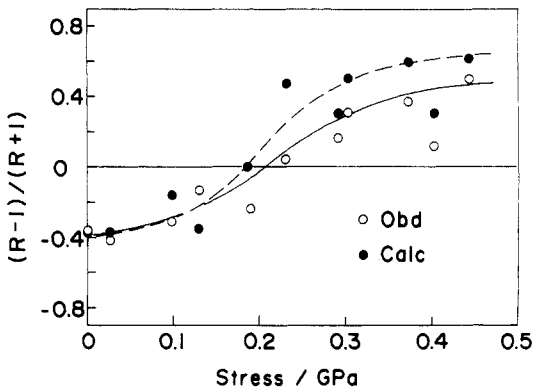

Figure 10. Plot of $(R - 1)/(R + 1)$ vs stress. $R = I_2/I_1$ where I_1 and I_2 are the integrated intensities of the bands 1 and 2.

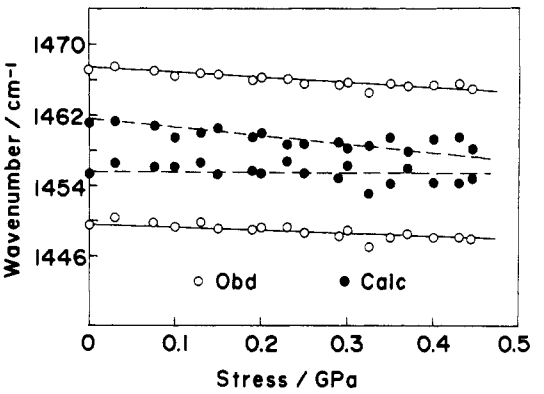

Figure 11. Stress dependence of peak frequencies of the coupled bands in the region 1450–1470 cm^{-1} (open circles). The solid circles represent the behavior of the unperturbed modes calculated from the data of open circles.

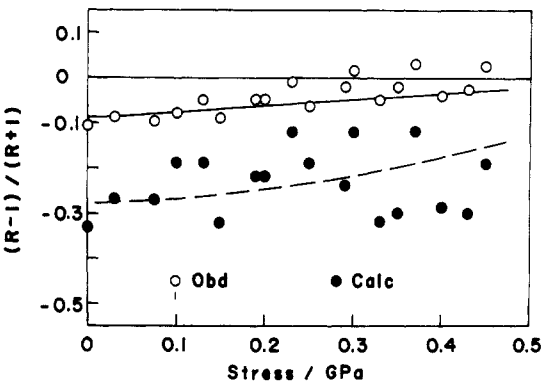

Figure 12. Plot of $(R - 1)/(R + 1)$ vs stress, where R is the ratio of the integrated intensity of the Raman band located near 1450 cm^{-1} to that of the band at ca. 1468 cm^{-1}.

where $\tilde{\nu}_1^0$ is assumed higher than $\tilde{\nu}_2^0$.

In order to evaluate the relative intensities I_1 and I_2 reasonably, the overlapped bands in the frequency regions 1180–1240 cm^{-1} and 1400–1500 cm^{-1} were separated numerically into components. In Figures 9–12, such peak frequencies and intensity ratios R, in a form of $(R - 1)/(R + 1)$, are plotted against stress, where the integrated intensities were used for I_1 and I_2. For a pair of 1220- and 1212-cm^{-1} bands, the intensity ratio R becomes unity for the stress $\sigma^* \approx 0.2$ GPa. Then, the perturbation energy $\tilde{W}_{12}$ was evaluated from the band separation at σ^* as

$$|\tilde{W}_{12}| = 4.0 \text{ cm}^{-1}$$

For a pair of 1468- and 1450-cm^{-1} bands, such a stress σ^* cannot be found in the experimental region. Then, fol-

lowing the process described above, the $|\tilde{W}_{12}|$ was estimated by a trial and error method:

$$|\tilde{W}_{12}| = 8.3 \text{ cm}^{-1}$$

Using these values of $|\tilde{W}_{12}|$ and the observed frequencies $\tilde{\nu}_1'$ and $\tilde{\nu}_2'$, the unperturbed frequencies $\tilde{\nu}_1^0$ and $\tilde{\nu}_2^0$ and the intensity ratio R were calculated. The calculated curves of $(R - 1)/(R + 1)$ shown in Figures 10 and 12 are considered to reproduce the observed data fairly well for the band pair 1220 and 1212 cm^{-1} but not so well for the pair 1468 and 1450 cm^{-1}. This may be due to the approximation that the vibrational coupling in the frequency region 1400–1500 cm^{-1} occurs between only two bands at 1468 and 1450 cm^{-1} and a residual component at 1422 cm^{-1} was neglected in the analysis. Strictly speaking we will have to take into account the coupling among the three vibrational modes. But as long as the vibrational frequency is concerned, the resultant $\tilde{\nu}_i^0$ will not be greatly affected by the present approximation.

As seen in Figures 9 and 11, the bands with $\tilde{\nu}^0 = 1217$ cm^{-1} and 1462 cm^{-1} are found to shift with stress, while those at 1214 and 1456 cm^{-1} do not shift so much. It may be reasonable to assign the bands at 1462 and 1217 cm^{-1} (for $\sigma = 0$ GPa) to the unperturbed ν(C=C) and δ(C—C=C) modes, respectively. The normal mode calculation described in the previous section supports also this conclusion.

As pointed out in the above section, the bands at 1450 and 1422 cm^{-1} may be assigned to the side-group modes and this assigment is supported also by their small frequency shift under tension. These bands are considered originally in an off-resonance state for the 632.8-nm excitation beam and show negligibly small contribution to the resonance Raman intensity. Through a vibrational coupling, the energy of the skeletal modes flows into the side group and then the side-group band has a detectable Raman intensity. At the same time the frequency position is also affected. But, as seen in Figures 9 and 11, the vibrational coupling seems relatively small compared with the case of polyTS.[5]

B. Infrared Spectral Change. As shown in Figure 4, the resonance Raman spectra of polyDCHD give only the information concerning the conjugated skeletal bonds of C=C and C≡C. The stretching mode of the skeletal C—C single bond is included in the Raman spectra only in a form coupled with C=C and C≡C stretching modes (see Figure 6 and Table I). Referring to the results of the normal-mode calculation stated above, we predict that the C—C stretching mode could be observed by means of the infrared spectra: the antisymmetric C—C stretching mode ν_{as}(C—C) belongs to the infrared-active B_u species and the vibrational coupling with the other modes is very small [the potential energy distribution is about 88% to ν_{as}(C—C) as shown in Table I]. It has been, however, difficult for a long time to prove such a prediction experimentally. This is because most of the infrared data for a series of PDA's reported so far were in a reflection spectral pattern which is difficult to analyze and also because, even in a transmission fashion, a detection of bands with a conventional dispersion-type infrared spectrophotometer is extremely difficult for a micron-sized single crystal of polyDCHD. Then we tried to utilize the Fourier transform infrared spectrophotometer (FTIR) and succeeded in the first measurement of the polarized infrared transmission spectra of polydiacetylene single crystal. Figure 13 shows the polarized FTIR spectra of a polyDCHD single crystal measured under free tension in the frequency region 500–3500 cm^{-1}. The infrared spectra are very complicated. By comparing them with the infrared spectra of carbazole

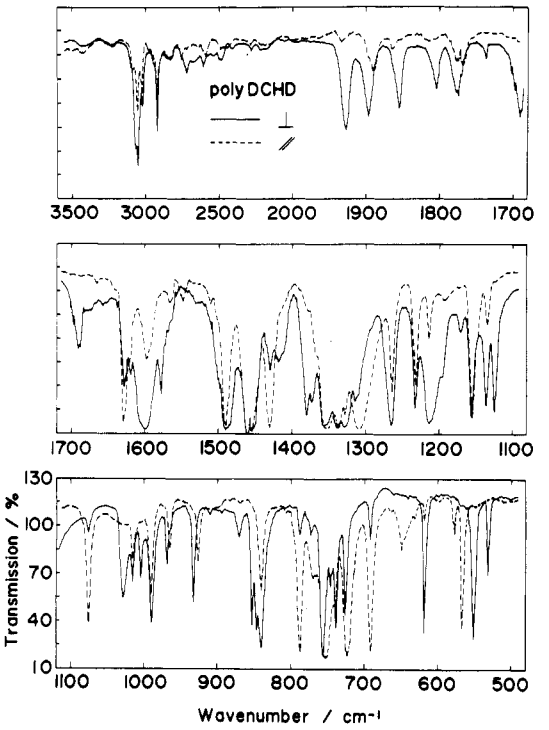

Figure 13. Polarized FTIR spectra of polyDCHD single crystal: (—) the electric vector of the incident IR beam is perpendicular to the chain axis; (---) the electric vector of the incident IR beam is parallel to the chain axis.

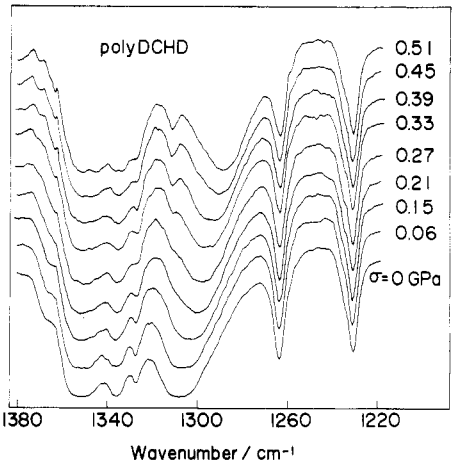

Figure 14. Stress dependence of the FTIR spectra (parallel polarization component) measured in the frequency region 1220–1380 cm^{-1}.

and *N*-ethylcarbazole, most of the bands are found to come from the side group. When the single crystal was stretched along the chain axis under the external tensile stress, as shown in Figure 14, only a parallel band at 1307 cm^{-1} was found to show a large low-frequency shift with an increase in stress (−31 cm^{-1}/GPa) and all the other bands did not show any detectable frequency shift. On the basis of the combined data of the normal mode analysis, the polarization character, and the experimental fact that only the 1307-cm^{-1} band shifts largely under tension, it may be possible to assign this 1307-cm^{-1} band to the skeletal C—C stretching mode ν_{as}(C—C). The other bands are assigned to local vibrational modes of such side branches as methylene and carbazolyl groups. The frequency value of 1307 cm^{-1} seems a little higher than the usually observed frequency of about 1100 cm^{-1} for the ν_{as}(C—C) mode. But as understood from the resonance between two types of structure, i.e., a diacetylene and a butatriene type,[14] the

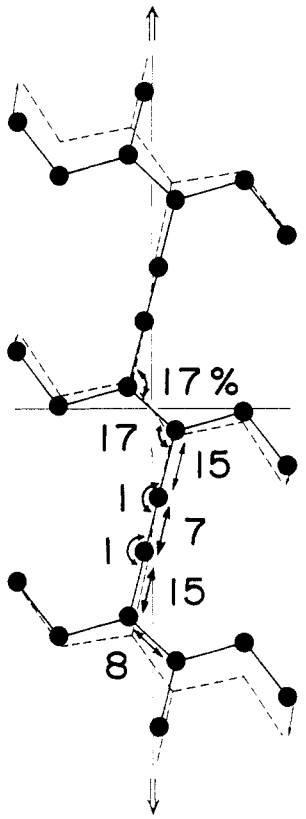

Figure 15. Atomic displacements and the potential energy distribution calculated for a polyDCHD single chain under the hypothetically large tensile strain of 10%. The solid and broken lines represent the undeformed and deformed conformations of the chain, respectively.

skeletal C—C bonds have the possibility of possessing some degree of double-bond character. This is supported from

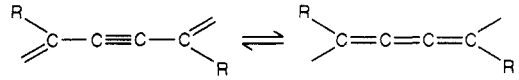

the X-ray structural analysis, which says that the skeletal C—C single bond length in polyDCHD is about 0.142 nm and appreciably shorter than the usual value of about 0.154 nm. The corresponding force constant K(C—C) was about 5.6×10^2 N m^{-1}, which is comparable to the value of K-(C═C), ca 5.1×10^2 N m^{-1}, and appreciably high compared with $3\text{–}4 \times 10^2$ N m^{-1} reported for the usual aliphatic compounds.

C. Stress-Induced Spectral Change and Molecular Deformation Mechanism of PolyDCHD Chain. Figure 15 shows the atomic displacements and potential energy distribution (PED) calculated for the deformed PDA chain, where the PED represents the distribution of the externally applied deformation energy to the internal coordinates such as bond length, bond angles, etc.[15] The PED to the ν(C≡C), ν(C—C), ν(C═C), and δ(C—C═C) modes are large. The linearly linked bonds of C—C≡C—C may be assumed as one virtual bond, which inclines about 14° from the vertical chain axis. Under tension, such a virtual bond is stretched and tends to rotate toward the vertical axis by opening the C—C═C bond angles. These deformation behaviors are consistent with the Raman and FTIR spectral data showing a large frequency shift of these modes. In other words, the theoretically predicted mechanical deformation mechanism of the PDA chain is supported experimentally by the vibrational spectroscopic measurement under tension.

Change in Raman and FTIR Spectra under Tension at Various Temperatures. As an example, Figure 16 shows the Raman spectral change under tension measured for the skeletal modes at 210 °C. In Figure 17 are shown the frequency shifts measured at various temperatures. It can be noticed here that the frequency shift becomes larger as the temperature is raised. For example, the frequency shift of the ν(C≡C) band is $\Delta\tilde{\nu}/\Delta\sigma \approx -40$ cm^{-1}/GPa at room temperature and −56 cm^{-1}/GPa at 210 °C. For the δ(C—C═C) mode, $\Delta\tilde{\nu}/\Delta\sigma \approx -9$ cm^{-1}/GPa at room temperature and −20 cm^{-1}/GPa at 210 °C. As in the case measured at room temperature, only the infrared-active ν_{as}(C—C) band is observed to shift largely in the infrared spectra measured at high temperature: the frequency shift factor $\Delta\tilde{\nu}/\Delta\sigma$ is about −33 cm^{-1}/GPa at 210 °C, a little larger than the room temperature value (−31 cm^{-1}/GPa).

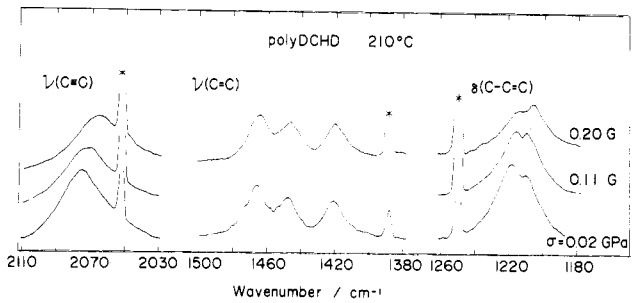

Figure 16. Stress dependence of the Raman spectra measured for the ν(C≡C), ν(C═C), and δ(C—C═C) bands of polyDCHD at 210 °C. Asterisks are due to the emission from a neon lamp.

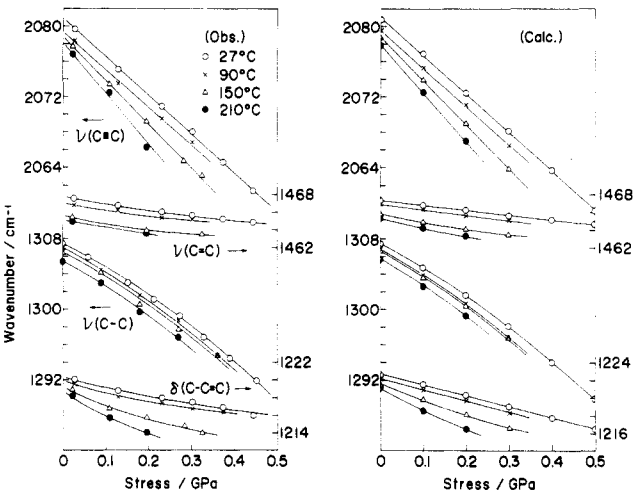

Figure 17. Comparison of the observed and calculated stress dependences of the vibrational frequencies of polyDCHD at various temperatures. (In the normal mode calculation, the observed frequencies were interpolated to the values at constant stress.)

Stress and Temperature Dependence of the Intramolecular Force Constants. Using the Raman and infrared spectral data measured under stress at the various temperatures, the force constants, as a function of stress and temperature, were determined so as to give good reproducibility of the vibrational frequencies. The stress dependences of the force constants K(C≡C), K(C═C), K(C—C), and H(C—C═C) at the various temperatures are illustrated in Figure 18. The force constants are found to decrease gradually with an increment of stress and temperature: for example, ΔK(C═C)/$\Delta\sigma$ = −1.0%/GPa, ΔK(C≡C)/$\Delta\sigma$ = −3.5%/GPa, ΔH(C—C═C)/$\Delta\sigma$ = −1.0%/GPa, and ΔH(C—C≡C)/$\Delta\sigma$ = 0%/GPa, at room temperature. The change in the force constant of the C—C single bond, estimated from the infrared data, is about −6.1%/GPa at room temperature. From these results we

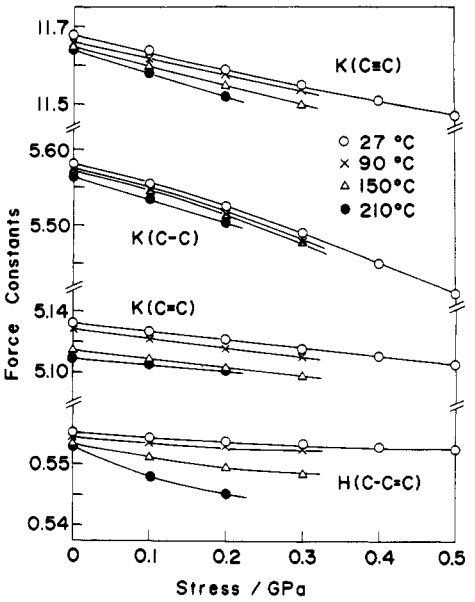

Figure 18. Stress dependence of intramolecular force constants for a polyDCHD single chain. The units are 10^2 N m^{-1} for K(C—C), K(C=C), and K(C≡C) and 10^2 N m rad^{-2} for H(C—C=C). (In the normal mode calculation, the observed frequencies were interpolated to the values at constant stress.)

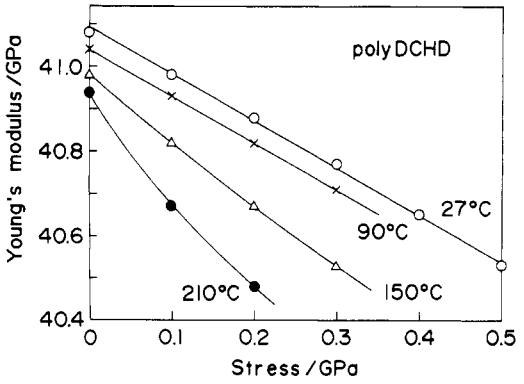

Figure 19. Stress dependence of Young's modulus calculated for a polyDCHD single chain at various temperatures.

may say that the mechanical anharmonicity of the C≡C and C—C stretching modes is very substantial compared with that of the other modes.

Stress and Temperature Dependence of Young's Modulus. Theoretical Young's modulus of the polyDCHD chain was calculated as a function of stress and temperature. In the calculation, only the force constants are assumed to change with stress and temperature, as determined above, and the geometrical change is ignored, i.e., the atomic positions are assumed to remain unchanged irrespective of the differently stressed state of the chain. The calculation was based on the lattice dynamical theory described in ref 8. The calculated modulus under free tension is 41.1 GPa at room temperature, in good agreement with the experimental values 43.2 GPa obtained from the stress–strain curve (Figure 21) and 46.6 GPa by the Brillouin scattering measurement.[16] In Figure 19, the calculated Young's modulus is plotted against stress. The modulus decreases as the applied stress is increased. Such a tendency becomes more prominent at higher temperature.

In order to ascertain the calculated results, we have measured Young's modulus of a polyDCHD single crystal as a function of stress and temperature. The measured stress–strain curves are reproduced in Figure 20, where the curve at room temperature is in good agreement with the

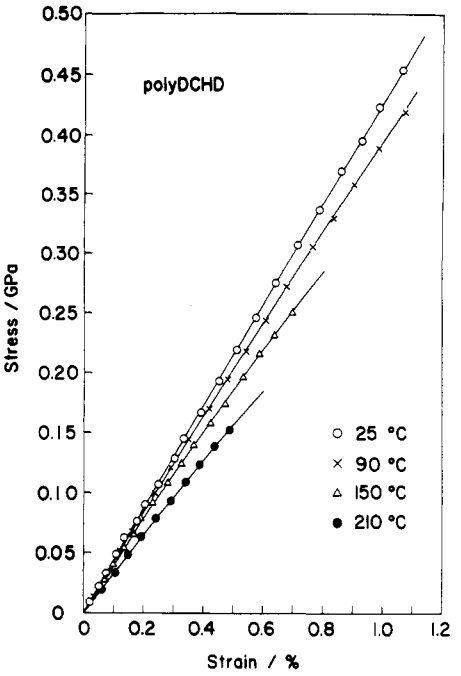

Figure 20. Stress–strain curves measured for a polyDCHD single crystal at various temperatures.

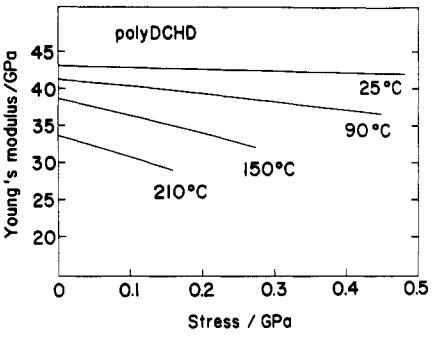

Figure 21. Stress dependence of Young's modulus of a polyDCHD single crystal measured at various temperatures.

data by Galiotis et al.[17] Young's modulus was estimated as follows: these data were fitted to the second-order polynomial through the least-squares method and then the modulus was obtained by differentiating this function with respect to strain at a particular position. In Figure 21 is plotted the stress dependence of the thus obtained Young's modulus at various temperatures. At room temperature, the decrease in modulus $\Delta E_l/E_l^0$ in the stress region 0–0.5 GPa is about $-1.0/43.2 = -2.3\%$, where E_l^0 is the modulus at a stress of 0 GPa. The corresponding calculated value is $-0.5/41.1 = -1\%$. The difference between them is too large to be neglected. The larger decrease in the calculated Young's modulus at higher temperature is qualitatively consistent with the observed result. Quantitatively, however, the observed modulus decreases more drastically than the calculated modulus as the temperature increases. For example, under free tension, the calculated decrease in modulus in the temperature range 27–210 °C is only about $-0.2/41.1 = -0.5\%$, while the observed value is about $-10/43 = -23.3\%$. As the stress is increased, the difference between them becomes more remarkable. One possible origin for such a large difference in the temperature dependence of Young's modulus between the observed and calculated ones may be related with an anharmonic vibration in the crystal lattice. As described in ref 18, Young's modulus along the chain direction at a temperature T is given as follows under a quasiharmonic approximation:

$$E^T \approx E^0 - kT\sum_l (\gamma_l)^2 \quad (7)$$

where E^0 is Young's modulus at room temperature and k is the Boltzmann constant. γ_l is the Grüneisen constant for the vibrational mode l subjected to the strain ϵ or stress σ and defined by

$$\gamma_l = -\frac{1}{\tilde{\nu}_l}\left(\frac{\partial \tilde{\nu}_l}{\partial \epsilon}\right) = -\frac{1}{\tilde{\nu}_l}\left(\frac{\partial \tilde{\nu}_l}{\partial \sigma}\right)E^T \quad (8)$$

Equation 7 expresses a decrease in modulus with increasing temperature. Using the shift factors ($\Delta\tilde{\nu}/\Delta\sigma$) observed for polyDCHD, the mode Grüneisen constant is evaluated as

$$\nu(C{\equiv}C) \qquad \gamma_l = 1.2$$
$$\nu(C{=}C) \qquad \gamma_l = 0.2$$
$$\nu(C{-}C) \qquad \gamma_l = 1.2$$
$$\delta(C{-}C{=}C) \qquad \gamma_l = 0.7$$

Thus a slope $\Delta E/\Delta T$ is obtained in a rough estimation as

$$\Delta E/\Delta T = -k\sum_l (\gamma_l)^2 \approx -9 \times 10^{-5}\ \mathrm{GPa/K}$$

where the temperature dependence of γ_l is assumed to be small.

Thus estimated $\Delta E/\Delta T$ is too small to interpret the observed temperature dependence of the modulus, suggesting that, in the variation of Young's modulus with temperature, the contribution of the bond stretching and bond angle deformation modes of the skeletal chain is negligibly small. In other words, we must search for other types of vibrational modes which govern the temperature behavior of the modulus at high weight. One possibility may be a skeletal torsional mode which could not be observed by the present Raman and IR measurements. In a previous paper,[7] we have developed a theory in which a decrease in the modulus with increasing temperature was interpreted on the basis of an idea of large-amplitude thermal fluctuation motion of the fully extended chain. The torsional modes around the skeletal bonds are considered to correlate with such a flexual chain motion. We are now trying to investigate how and to what extent this vibrational mode of τ(skeletal) affects the temperature and stress dependences of Young's modulus of the PDA chain.

Registry No. DCHD (homopolymer), 69289-06-1; DCHD (SRU), 66336-91-2.

References and Notes

(1) Clements, J.; Jakeways, R.; Ward, I. M. *Polymer* **1978**, *19*, 639.
(2) Geil, P. H. *Polym. Colloq. Kyoto* **1977**, 48. Hasegawa, H.; Hagerling, C. W.; Hoffman, R. W.; Geil, P. H. *Polym. Prepr. Jpn.* **1979**, *28*, 1870.
(3) Wegner, G. *Pure Appl. Chem.* **1977**, *49*, 443.
(4) Mitra, V. K.; Risen, W.; Baughman, R. H. *J. Chem. Phys.* **1977**, *66*, 2731.
(5) Batchelder, D. N.; Bloor, D. *J. Polym. Sci., Polym. Phys. Ed.* **1979**, *17*, 569.
(6) Galiotis, C.; Young, R. J.; Batchelder, D. N. *J. Polym. Sci., Polym. Phys. Ed.* **1983**, *21*, 2483.
(7) Ii, T.; Tashiro, K.; Kobayashi, M.; Tadokoro, H. *Macromolecules* **1987**, *20*, 552.
(8) Tashiro, K.; Kobayashi, M.; Tadokoro, H. *Macromolecules* **1977**, *10*, 731.
(9) Yee, K. C.; Chance, R. R. *J. Polym. Sci., Polym. Phys. Ed.* **1978**, *16*, 431.
(10) Kennedy, R. J.; Chalmers, I. F.; Bloor, D. *Makromol. Chem., Rapid Commun.* **1980**, *1*, 357.
(11) Apgar, P. A.; Yee, K. C. *Acta Crystallogr., Sect. B: Struct. Crystallogr. Cryst. Chem.* **1978**, *B34*, 957.
(12) Lewis, W. F.; Batchelder, D. N. *Chem. Phys. Lett.* **1979**, *60*, 232.
(13) Tadokoro, H. *Structure of Crystalline Polymers*; Wiley-Interscience: New York, 1979.
(14) Enkelmann, V. *Adv. Polym. Sci.* **1984**, *63*, 91.
(15) Tashiro, K.; Kobayashi, M.; Tadokoro, H. *Macromolecules* **1977**, *10*, 413.
(16) Enkelmann, V.; Leyrer, R. J.; Schleier, G.; Wegner, G. *J. Mater. Sci.* **1980**, *15*, 168.
(17) Galiotis, C.; Reed, R. T.; Yeung, P. H. G.; Young, R. J.; Chalmers, I. F.; Bloor, D. *J. Polym. Sci., Polym. Phys. Ed.* **1984**, *22*, 1589.
(18) Tashiro, K.; Kobayashi, M.; Tadokoro, H. *Polym. J.*, in press.

Structure Analysis of Polyisobutylene Based on the Whole-Pattern Fiber Diffraction Method. 1. Intensity Distribution Functions

Pio Iannelli and Attilio Immirzi*

Dipartimento di Fisica, Università di Salerno, I-84100 Salerno, Italy.

Received January 6, 1988; Revised Manuscript Received June 8, 1988

ABSTRACT: The structure of polyisobutylene crystallized under stretching has been used to verify the feasibility of the "whole-pattern" approach to structure refinement problems based on the X-ray fiber diffraction pattern, a novel procedure recently introduced by us. This paper is concerned specifically with the analysis of the resolved peaks of the spectrum for establishing empirically appropriate intensity distribution functions by means of parametrized functions and the dependence of the parameters themselves on the positions of the peaks on the spectrum.

Introduction

In previous papers[1,2] we have introduced a novel method for performing crystal structure refinements of fibrous materials which consists of using, instead of "integrated" diffraction intensities, the "whole diffraction pattern" (dp). This new approach can be considered an extension of Rietveld's method[3,4] from the powder case (one-dimensional dp) to the fiber case (two-dimensional dp).

At present we have considered the X-ray dp recorded by photographic techniques and digitized by a photoscan instrument. The method is potentially applicable, however, also with other recording techniques (e.g., counter techniques, X-ray television cameras, etc.) as well as to other radiation sources such as synchrotron radiation.

A basic question which arises is the choice of proper distribution functions for the diffracted intensity in *two directions*: along the increasing Bragg angle and along the constant Bragg angle directions. As discussed in a previous paper[1] a possible choice is to refer the intensity to the proper pair of curvilinear film coordinates (ρ,τ lines; τ are

0024-9297/89/2222-0196$01.50/0